Design and control of Proportional–Resonant controller based Photovoltaic power conditioning system

Conference Paper · October 2009

DOI: 10.1109/ECCE.2009.5316374 · Source: IEEE Xplore

3 authors:

Hanju Cha
Chungnam National University
57 PUBLICATIONS **590** CITATIONS
SEE PROFILE

Trung-Kien Vu
Hex Power System, Korea
28 PUBLICATIONS **341** CITATIONS
SEE PROFILE

Jae-Eon Kim
Chungbuk National University
43 PUBLICATIONS **454** CITATIONS
SEE PROFILE

Design and Control of Proportional-Resonant Controller Based Photovoltaic Power Conditioning System

Hanju Cha*, Trung-Kien Vu* and Jae-Eon Kim**

*Chungnam National University/ Department of Electrical Engineering, Daejon, Korea
**Chungbuk National University/ Department of Electrical Engineering, Cheongju, Korea

***Abstract* -- This paper presents a current control technique for a single-phase grid-connected DC/AC inverter which is used in Photovoltaic power conditioning system (PV PCS). A Proportional - Resonant (PR) controller is used for replacing the conventional Proportional - Integral (PI) controller in this system. By comparison with the conventional PI control method, the PR control can introduce an infinite gain at the fundamental frequency and hence can achieve zero steady-state error. A theoretical analysis of the PR controller is presented and verified by experiment. Furthermore, a pseudo synchronous d-q transformation is employed in current control scheme and an all-pass filter based single-phase digital phase-locked loop (PLL) is introduced to detect the phase of grid voltage. Based on the theoretical analysis, the control strategy is implemented on a 32-bit fixed-point TMS320F2812 DSP and tested in a 3kW prototype PV PCS. Simulation and experimental verify the high performance of the implemented control scheme.**

***Index Terms*—Dc/Ac inverter, Photovoltaic, Proportional-Resonance (PR) controller.**

I. INTRODUCTION

Nowadays, more and more concern of photovoltaic (PV) energy has been focused on interconnection between the PV power systems and the grid. Generally, the grid-connected PV power systems mainly consist of a boost DC/DC converter and a DC/AC inverter. The DC/AC inverter, either single or three-phase designs, can be considered as the core of the whole system because of an important role in grid-connected operation.

Although current and voltage control schemes are possible and implementable, the current control principle is generally preferred for its excellent dynamic characteristics and its inherent over-current limitation capabilities. Several methods have been proposed in the literature for the control of such inverters [1]-[3]. As for predictive control, it depends on the accuracy of both the system model and the reference current prediction [1]-[2]. While the hysteresis control is simple and robust, it has major drawbacks in variable switching rate, current error of twice the hysteresis band, and high frequency limited cycle operation [3]. Furthermore there is an unsolved problem of steady-state error in those current control strategies mentioned above.

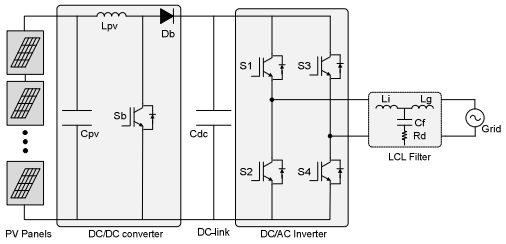

Fig. 1 Block diagram of single-phase grid connected PV PCS

PV power conditioning system (PV PCS), as depicted in Figure 1, is usually built with Proportional-Integral (PI) controller in current control scheme [4]. In order to achieve zero steady-state error, a Proportional-Resonant (PR) controller based current control which is used to replace the conventional PI controller is implemented for the grid-connected DC/AC inverter in the PV PCS. Compared with the conventional PI control, the introduced PR control can overcome two well-known drawbacks of PI control: inability to track a sinusoidal reference with zero steady-state error and poor disturbance rejection capability. Due to an infinite gain at the fundamental frequency, the PR controller can achieve the high performance in both the sinusoidal reference tracking and the disturbance rejection.

II. CURRENT CONTROL SCHEME FOR SINGLE-PHASE GRID-CONNECTED DC/AC INVERTER

A. Current control with PR controller

The ideal resonant controller, which is given by (1), can be mathematically derived by transforming an ideal synchronous frame PI controller to the stationary frame and achieves infinite gain at the AC frequency of ω_0 as shown in Fig. 2(a) to force the steady-state voltage error to zero, and no phase shift and gain at other frequencies. For K_p, it is tuned in the same way as for a PI controller.

Unfortunately, the ideal PR controller acts like a network with an infinite quality factor, which is hard to implement the PR controller in reality. Firstly, the infinite gain introduced by PR controller leads to an infinite quality factor which cannot be achieved in either analog or digital system.

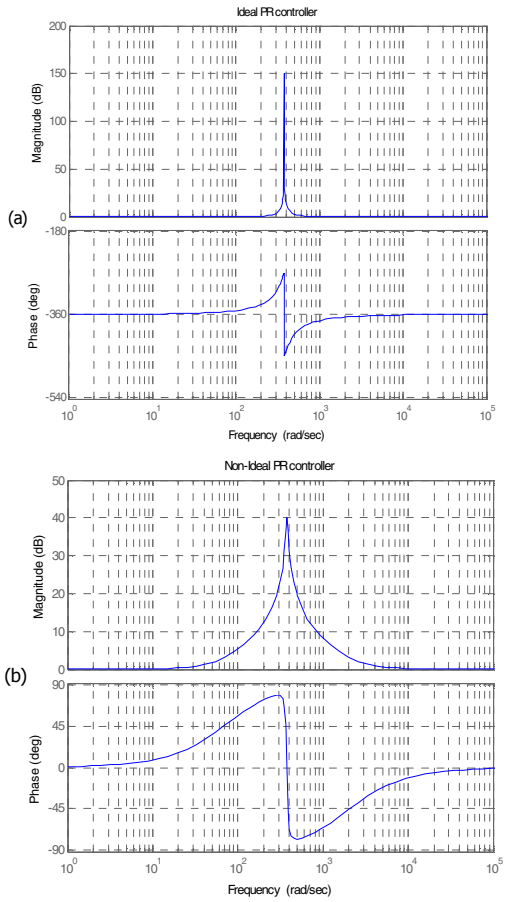

Fig. 2 Frequency responses of (a) ideal PR controller and (b) non-ideal PR controller with K_p=1, K_i=100, ω_{cut}=10 (rad/s).

Secondly, the gain of PR controller is much reduced at other frequencies and it is no adequate to eliminate harmonic influence caused by grid voltage. Therefore, an approximating ideal (non-ideal) PR controller, is given by (2), using a high-gain low-pass filter is used to solve the problems mentioned above [5]-[7].

$$G_S(s) = K_p + \frac{2K_i s}{s^2 + \omega_0^2} \tag{1}$$

$$G_S(s) = K_p + \frac{2K_i \omega_{cut} s}{s^2 + 2\omega_{cut} s + \omega_0^2} \tag{2}$$

where K_p, K_i are gain constants; ω_0 (= $2\pi\times60$rad/s) is grid frequency and ω_{cut} is cutoff frequency.

The frequency response of (2) is shown in Fig. 2(b), where the resonant peak now has a finite gain of 40 dB which is satisfactorily high for eliminating the voltage tracking error.

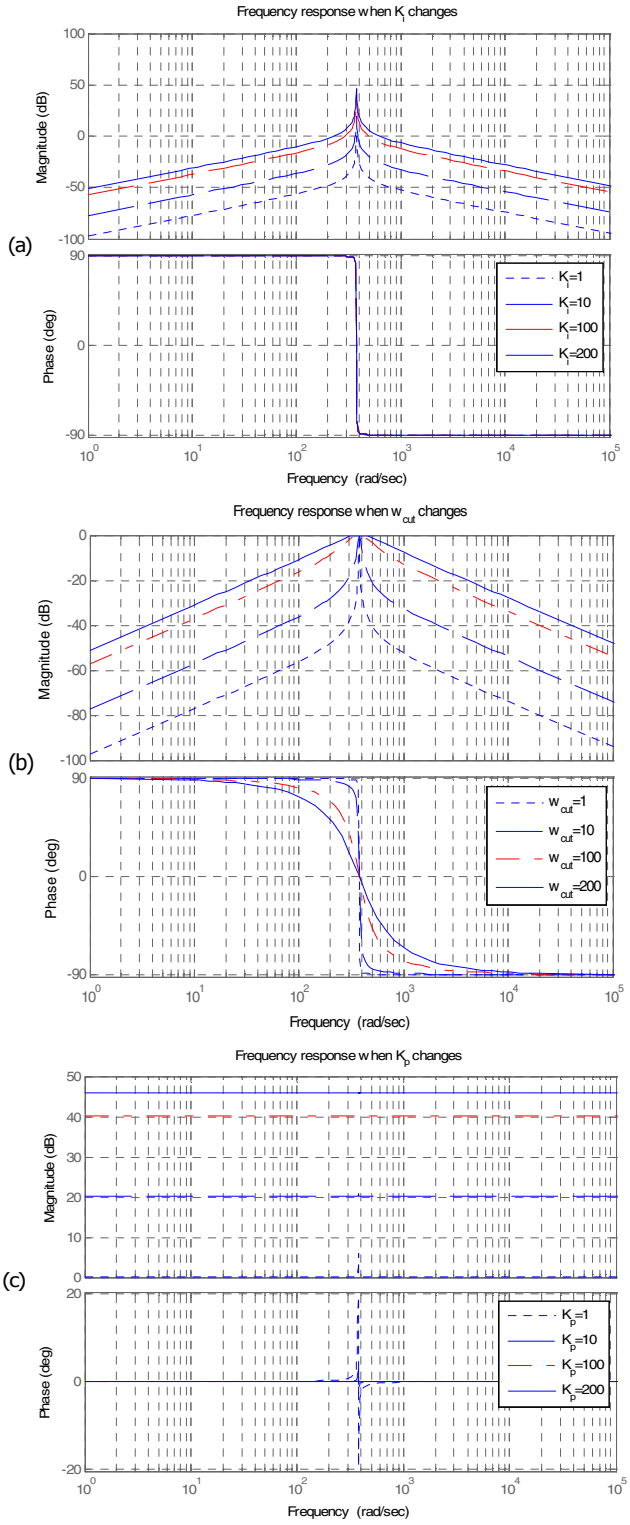

Fig. 3 Frequency responses of non-ideal PR controller when (a) K_i changes, (b) ω_c changes and (c) K_p changes.

In addition, a wider bandwidth is observed around the resonant frequency, which minimizes the sensitivity of the

controller to slight grid frequency variations. At other harmonic frequencies, the response of the non-ideal PR controller is comparable to that of the ideal PR controller.

From (2), it can be seen that there are three parameters in the PR controller including K_p, K_i and ω_{cut}. For simplicity of analysis, we assume two of these parameters to be constant, and then the effect of changes in the third parameter can be easily observed.

Assuming $K_p = 0$, $\omega_{cut} = 1$, the change of K_i has no effect on the bandwidth but the gain of the controller as shown in Fig. 3(a). The magnitude of PR controller gain increases while K_i added.

Assuming $K_p = 0$, $K_i = 1$, the change of ω_{cut} has effects on both the magnitude and the phase of the controller as shown in Fig. 3(b). The magnitude and the phase increase when ω_{cut} increases, but the same gain can be achieved at the resonant frequency of the PR controller with adjustment of ω_{cut}.

Finally, as shown in Fig. 3(c), when K_p is added, the magnitude of PR regulator increases but has a peak value at the resonant frequency. But the phase magnitude decreases when K_p is added. It means that the harmonic impedance increases as K_p increases, and then the higher K_p can lead to a relatively low harmonic component. The value of K_p can be chosen to make sure that the system can achieve high performance in the sinusoidal reference tracking as well as the disturbance rejection.

Based on the theory analysis, in this paper, the PR controller gains are chosen as: $K_p = 15$, $K_i = 200$ and $\omega_{cut} = 15$(rad/s).

Fig. 4 shows the block diagram of current control scheme in the single-phase PV PCS [4].

In single-phase PV PCS, since the series L-filter achieves low attenuation of the inverter switching components, a capacitor (as a shunt element) is needed to further attenuate the switching frequency components. This shunt component must be selected to produce a low reactance at the switching frequency. But within the control frequency range, this element must present high magnitude impedance. But a very high capacitance is not recommended since the system may face with inrush current, high current fed on capacitor at the fundamental frequency, resonance phenomenon at the grid side, etc. If a system is connected to the grid via LC-filter, the resonance frequency varies over time as the inductance value of the grid [8]. The LCL-filter, as shown in Fig. 4, can provide a better decoupling between the filter and the grid impedance. A lower ripple current distortion across the grid-side inductor since the current ripple is reduced by the capacitor.

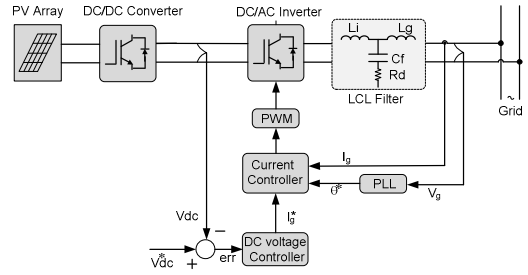

Fig. 4 Current control scheme for the single-phase PV PCS

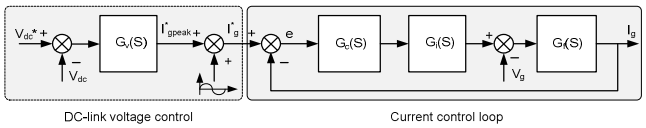

Fig. 5 Block diagram of the control loops

LCL-filter can provide a good attenuation ratio even with small L and C values. However, the three-order LCL-filter design needs to consider various constraints, such as the resonance phenomenon, the current ripple through inductors, the total impedance of the filter, the current harmonics attenuation at switching frequency and the reactive power absorbed by capacitor, etc.

The equivalent representation of the single-phase grid connected inverter with current regulation system can be obtained as shown in Fig. 5.

The relationship between input and output of current control loop is:

$$I_g = H_a(s)I_g^* + H_b(s)V_g \tag{3}$$

$$H_a(s) = \frac{I_g}{I_g^*} = \frac{G_c(s)G_i(s)G_f(s)}{1 + G_c(s)G_i(s)G_f(s)} \tag{4}$$

$$H_b(s) = \frac{I_g}{V_g} = \frac{G_f(s)}{1 + G_c(s)G_i(s)G_f(s)} \tag{5}$$

where $G_c(s)$ is the transfer function of the controller. $G_c(s)$ is shown in (2) in case of PR controller and $G_c(s) = K_p + \frac{K_i}{s}$ in case of PI controller; $G_i(s) = K$ is the transfer function of the inverter. Assuming the switching frequency is high enough to neglect the inverter dynamics, the PWM inverter can be represented by a gain for simplicity of analysis (due to relatively high switching frequency); $G_f(s) = \frac{R_d C_f s + 1}{L_i L_g C_f s^3 + (L_i + L_g) R_d C_f s^2 + (L_i + L_g)s}$ is the transfer function of LCL filter with damping resistor and

resonant frequency can be calculated as $\omega_{res}=\sqrt{\frac{L_i+L_g}{L_iL_gC_f}}$ [9].

As shown in (3), the output current depends on both the reference current and the grid voltage. In steady state, because the PI controller has a finite gain at the fundamental frequency, the second term of (3) cannot be neglected. However, PR controller introduces an infinite gain, then the first term approaches the inverter current reference and the second term approaches zero. Hence, the PR controller can achieve the zero steady-state error of the controlled inductor current.

The closed-loop transfer function of the current control system depicted in Fig. 5 is given by (6) in case of PI controller and is given by (7) in case of PR controller.

$$H_d(s)=\frac{K\left[R_dC_fK_ps^2+\left(K_p+K_iR_dC_f\right)s+K_i\right]}{L_iL_gC_fs^4+\left(L_i+L_g\right)C_fR_ds^3+\left(L_i+L_g+K_pKC_fR_d\right)s^2+\left(K_p+K_iR_dC_f\right)Ks+KK_i} \quad (6)$$

$$H_a(s)=\frac{K\left\{K_pR_dC_fs^3+\left[K_p+2\left(K_p+K_i\right)\omega_{cut}R_dC_f\right]s^2+\left[2\left(K_p+K_i\right)\omega_{cut}+K_pR_dC_f\omega_0^2\right]s+K_p\omega_0^2\right\}}{D_5s^5+D_4s^4+D_3s^3+D_2s^2+D_1s+D_0} \quad (7)$$

where

$$D_5=L_iL_gC_f \quad (8)$$

$$D_4=\left(L_i+L_g\right)C_fR_d+2L_iL_gC_f\omega_c \quad (9)$$

$$D_3=\left(L_i+L_g\right)\left(1+2\omega_cC_fR_d\right)+L_iL_gC_f\omega_0^2+KK_pC_fR_d \quad (10)$$

$$D_2=\left(L_i+L_g\right)\left(2\omega_c+C_fR_d\omega_0^2\right)+KK_p+2\left(K_i+K_p\right)KC_fR_d\omega_c \quad (11)$$

$$D_1=\left(L_i+L_g\right)\omega_0^2+KK_pC_fR_d\omega_0^2+2\left(K_i+K_p\right)K\omega_c \quad (12)$$

$$D_0=KK_p\omega_0^2 \quad (13)$$

Fig. 6 shows the bode diagram of closed-loop system in both PI and PR controller cases. As shown in Fig. 6, the PR controller can introduce an infinite gain at the fundamental frequency.

B. Implementation of PR controller in fixed-point DSP

By applying the bilinear transformation and substituting

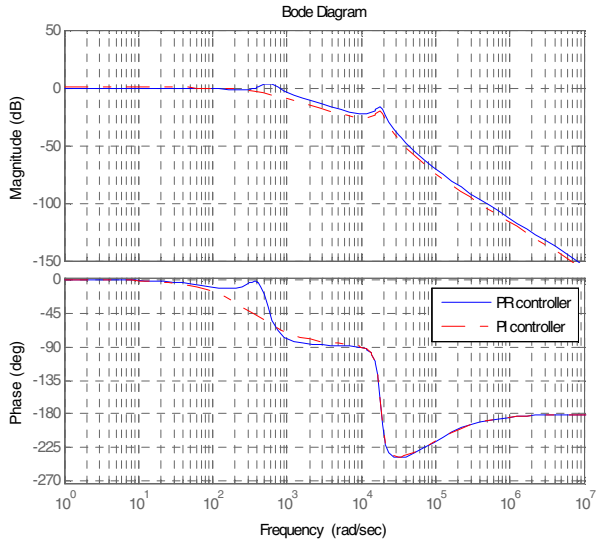

Fig. 6 Bode diagram of closed-loop transfer function using PI (K_p=10, K_i=50) and PR (K_p=15,K_i=200,ω_{cut}=15) controllers

$s=\frac{2}{T_S}\frac{1-z^{-1}}{1+z^{-1}}$ into (2), the discrete transfer function of the PR controller can be given by (14).

Or:

$$G_s(z)=\frac{n_0+n_1z^{-1}+n_2z^{-2}}{1+d_1z^{-1}+d_2z^{-2}} \quad (14)$$

where T_s is the sampling time and

$$n_0=\frac{\left(4+4T_s\omega_{cut}+\omega_0^2T_s^2\right)K_p+4K_iT_s\omega_{cut}}{4+4T_s\omega_{cut}+\omega_0^2T_s^2} \quad (15)$$

$$n_1=\frac{\left(2\omega_0^2T_s^2-8\right)K_p}{4+4T_s\omega_{cut}+\omega_0^2T_s^2} \quad (16)$$

$$n_2=\frac{\left(4-4T_s\omega_{cut}+\omega_0^2T_s^2\right)K_p-4K_iT_s\omega_{cut}}{4+4T_s\omega_{cut}+\omega_0^2T_s^2} \quad (17)$$

$$d_1=\frac{2\omega_0^2T_s^2-8}{4+4T_s\omega_{cut}+\omega_0^2T_s^2} \quad (18)$$

$$d_2=\frac{4-4T_s\omega_{cut}+\omega_0^2T_s^2}{4+4T_s\omega_{cut}+\omega_0^2T_s^2} \quad (19)$$

In this paper, $G_s(z)$ is implemented with a 32-bit fixed point DSP TMS320F2812. The discrete equation is given as:

$$y(k)=n_0u(k)+n_1u(k-1)+n_2u(k-2)-d_1y(k-1)-d_2y(k-2) \quad (20)$$

where y(k) is the output of the PR controller and u(k) is the current error input.

C. Single-phase digital phase-locked loop

In this paper, a single-phase digital phase-locked loop (DPLL) is implemented by making a virtual orthogonal voltage, which is delayed by 90° from the measured grid voltage and is generated by passing through an all-pass filter as shown in Fig. 7. The phase detection time of DPLL method is faster than conventional zero crossing detection method. The all-pass filter transfer function is given by:

$$H_{PLL}(s)=\frac{\omega-s}{\omega+s} \quad (21)$$

Substituting $s=\frac{2}{T_S}\frac{1-z^{-1}}{1+z^{-1}}$ into (21) yields:

$$H_{PLL}(s)=\frac{\omega T_S-2+(\omega T_S+2)z^{-1}}{\omega T_S+2+(\omega T_S-2)z^{-1}} \quad (22)$$

Hence, the virtual voltage which is generated from the measured grid voltage can be implemented by the following discrete difference equation:

$$y(k)=\alpha u(k)+u(k-1)-\alpha y(k-1) \quad (23)$$

where $\alpha=\frac{\omega T_S-2}{\omega T_S+2}$.

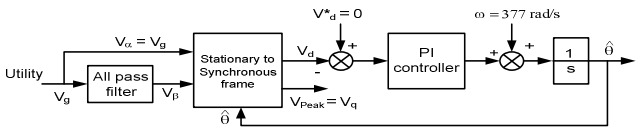

Fig. 7 Digital phase-locked loop

In Fig. 7, the grid voltage becomes α-component of stationary reference frame while β-component is a virtual voltage through the aforementioned all-pass filter. And then, the stationary reference frame αβ-components are converted to the synchronous reference frame dq-components, where d-component denotes a phase difference between grid voltage phase and estimated one.

In addition to the phase estimation, the instantaneous grid voltage peak can be calculated by considering it is the same as q-component.

III. Simulation Results

Fig. 8 shows the single-phase grid-connected DC/AC inverter model using Matlab/Simulink. The parameters used in simulation are listed in Table 1.

The performance of the DPLL using all-pass filter is depicted in Fig. 9, where the grid component becomes α-component and the β-component is generated by making a virtual voltage, which is delayed by 90◦ from the measured grid component.

The grid currents in stationary reference frame and in synchronous reference frame as shown in Fig. 9(a) and (b), respectively. The grid voltages in stationary reference frame and in the synchronous reference frame voltages are shown in Fig. 9(c) and (d), respectively. And the grid phase angle is shown in Fig. 9(e). All waveforms are in phase.

TABLE 1
PV PCCS PARAMETERS

Grid voltage	220V (RMS) 60Hz
DC bus voltage	400V
Inverter-side filter inductor L_i	2mH
Filter capacitor C_f	5μF
Filter damping resistor R_d	2.5Ω
Grid-side filter inductor L_g	0.86mH
Switching frequency	10KHz

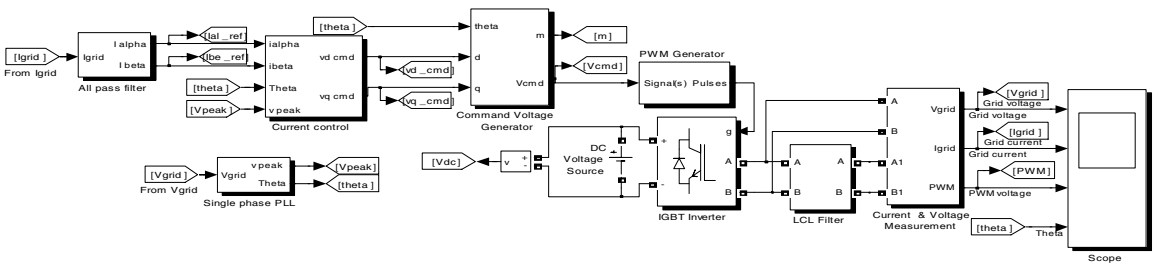

Fig. 8 Matlab/Simulink model of single-phase grid-connected DC/AC inverter

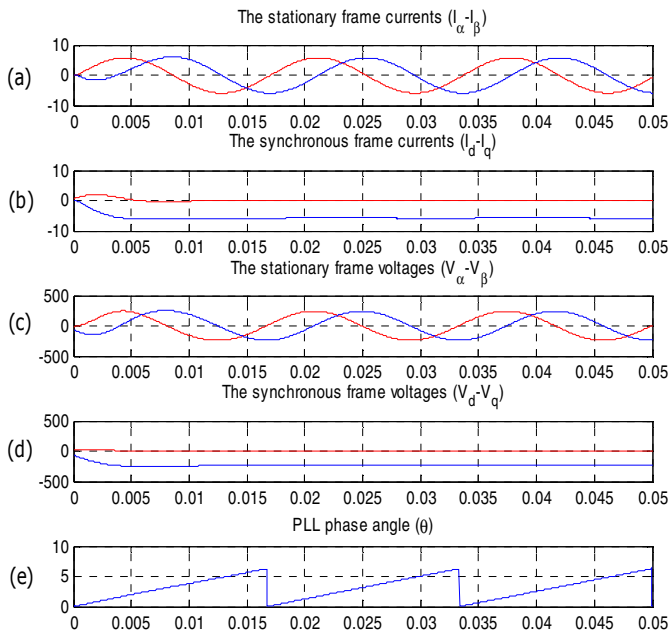

Fig. 9 Phase-locked loop operation

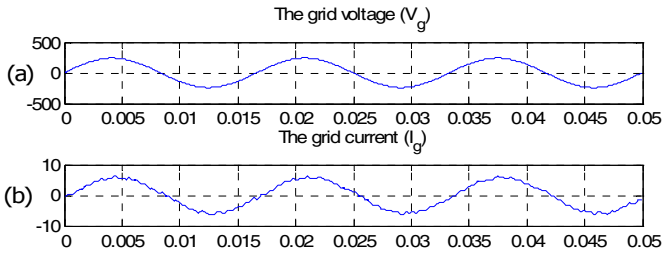

Fig. 10 Grid voltage and current using PR controller

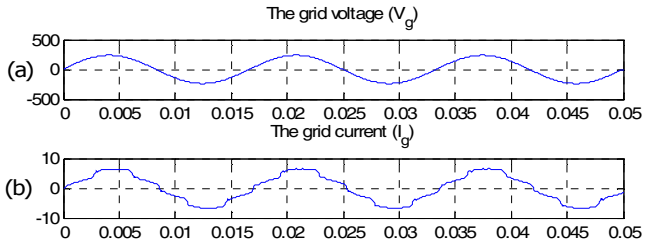

Fig. 11 Grid voltage and current using PI controller

Fig. 10 and Fig. 11 show the simulation responses of the control system by using the PR and PI controller, respectively. Fig. 10(a) and (b) show the grid voltage and grid current using PR controller, respectively. The grid voltage and current using the PI controller are shown in Fig. 11(a) and (b), respectively.

Fig. 12 and Fig. 13 show the frequency analysis of the grid current and its THD value by using the PR and PI controller, respectively.

The simulation results show that the PR controller can track the sinusoidal reference and mitigate the harmonics better than PI controller. It is noted that all waveforms are in phase.

IV. Experimental Results

The overall system of the 3kW PV PCS with grid connection, as shown in Fig. 14, is implemented fully in software adopting a 32-bit fixed-point DSP TMS320F2812. The PR controller for the inverter is implemented in software, and the PWM pulses are generated through the internal pulse generator of the DSP.

Voltage and current signals are measured by using the 12-bit resolution of internal analog-to-digital converter in the DSP. Also a four-channel 8-bit digital-to-analog converter has been used for debugging. The switching frequency of the inverter is chosen to 10 kHz and the dead-time is 3μs. The experimental results of the PV PCS are shown in Fig. 15 - Fig.19.

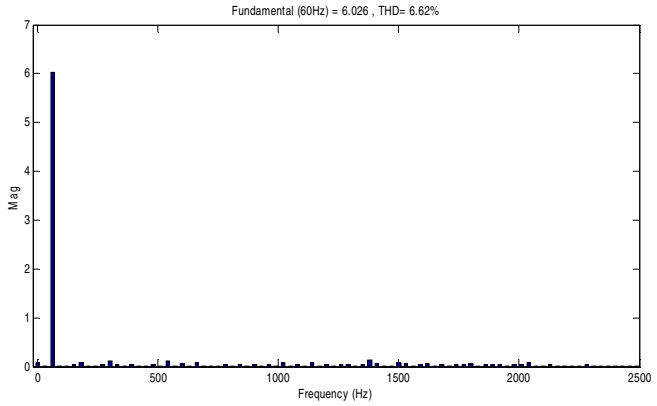

Fig. 12 FFT analysis and THD value of grid current by using PR controller

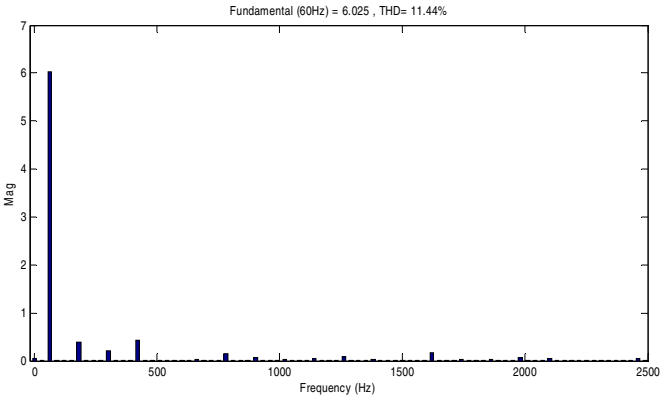

Fig. 13 FFT analysis and THD value of grid current by using PI controller

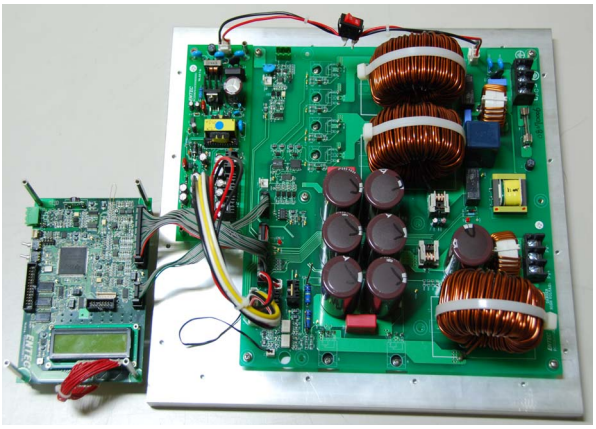

Fig. 14 Prototype of the implemented 3kW PV PCS

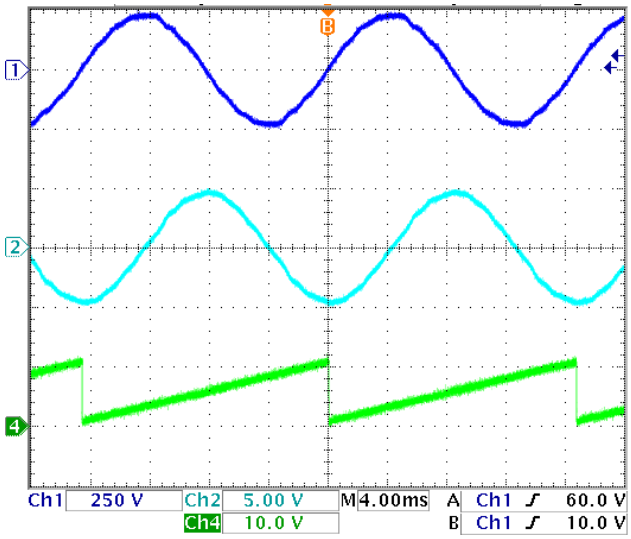

Fig. 15 Digital Phase-Locked Loop implementation results

Fig. 15 shows the implementation of the DPLL, where channel 1 shows the grid voltage (250V/div), channel 2 shows the calculated β-component of the grid voltage, that is generated by the all-pass filter and the phase angle is measured at channel 4. It is noted that all results are in phase.

Fig. 16 shows grid voltage in channel 1 (250V/div) and grid current in channel 4 (10A/div) by using the PR controller. It can be seen that the grid current waveform is nearly perfect sinusoid. It is noted that the experimental results show a good agreement with the simulation results and both waveforms are in phase.

On the other hand, the experimental results based on the conventional PI control are also obtained and shown in Fig. 17, with the same scales as Fig. 16. The frequency analysis and THD values of grid current using the PR and PI controller are shown in Fig. 18 and Fig. 19, respectively.

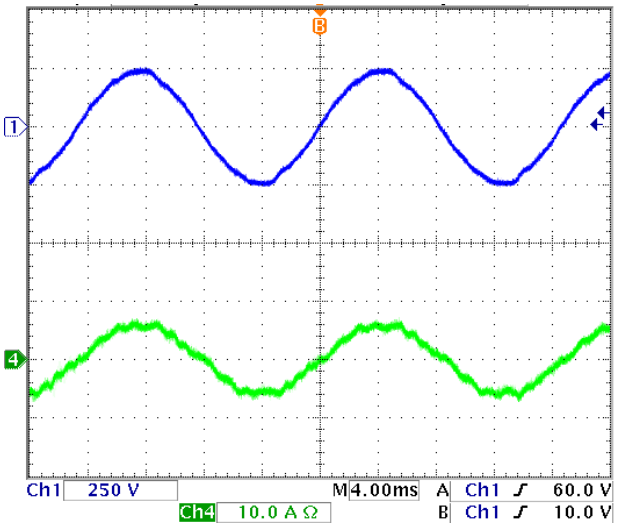

Fig. 16 Grid voltage and current implementation results with PR controller

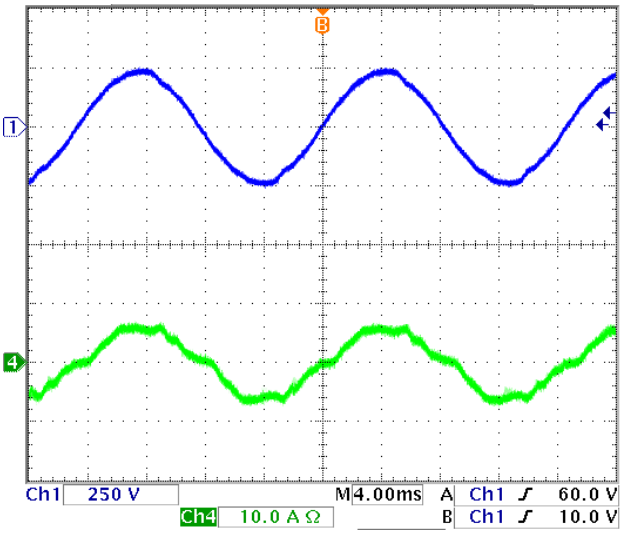

Fig. 17 Grid voltage and current implementation results with PI controller

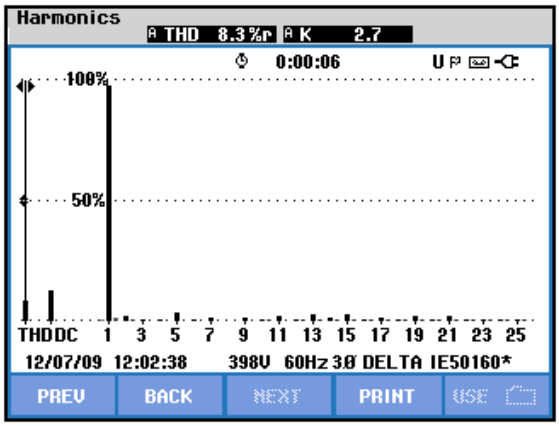

Fig.18. THD value of grid current implemented with PR controller

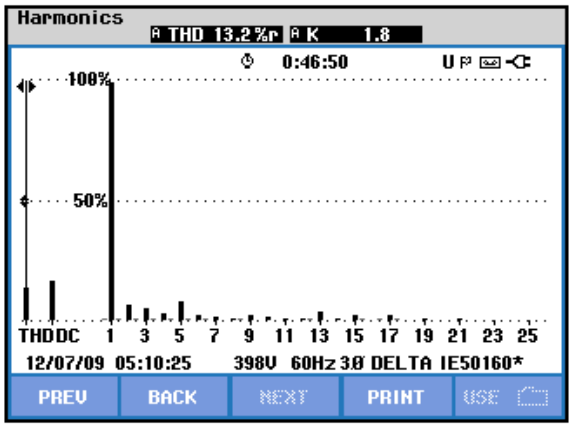

Fig.19. THD value of grid current implemented with PI controller

Compared with all the experimental results mentioned above, it is can be shown that the implementation of the PR control scheme can achieve the steady-state performance better than the conventional PI control scheme in DC/AC inverter control scheme of this PV PCS. Experimental results that the PR control can overcome drawbacks of PI control: inability to track a sinusoidal reference with zero steady-state error and poor disturbance rejection capability.

V. CONCLUSION

In this paper, a current based control scheme has been presented for a single-phase grid-connected DC/AC inverter in PV PCS with the PR controller. The modulation and control strategy is simulated by using Matlab/Simulink and implemented by using the 32-bit fixed-point DSP TMS320F2812. The theoretical analysis has been performed to enable single-phase grid-connected DC/AC inverter system to achieve the high performance and experimental results of a 3kW PV PCS prototype have verified the performance of the system. Simulation and experimental results show that the PR controller can overcome drawbacks of PI controller: inability to track a sinusoidal reference with zero steady-state error and poor disturbance rejection capability.

REFERENCES

[1] A. Kotsopoulos, J. L. Duart, M.A.M Hendrix, "A predictive control scheme for DC voltage and AC current in grid-connected photovoltaic inverters with minimum DC link capacitance", in *The 27th annual Conference of the IEEE Industrial Electronics Society*, vol.3, pp. 1994-1999, 2001.

[2] D. G. Holmes and D. A. Martin, "Implementation of a direct digital predictive current controller for single and three phase voltage source inverters", in *Proc. 1996 IEEE IAS Annu. Meeting*, pp. 906–913.

[3] R. D. Lorenz, T. A. Lipo, and D. W. Novotny, "Motion control with induction motors", in *Proc. 1994 IEEE*, vol. 82, iss. 8, pp. 1215-1240.

[4] Cha, Hanju, Lee, Sanghoey, "Design and Implementation of Photovoltaic Power Conditioning System Using a Current Based Maximum Power Point Tracking", in *Industry Application Society Annual Meeting*, pp. 1-5, Oct. 2008.

[5] Guo Xiaoqiang, Zhao Qinglin and Wu Weiyang 'A Single-Phase Grid-Connected Inverter System With Zero Steady-State Error', in *CES/IEEE 5th International Power Electronics and Motion Control Conference*, 2006, vol. 1, pp. 1-5, Aug. 2006.

[6] Zmood, D.N.; Holmes, D.G.; Bode, G., "Frequency domain analysis of three phase linear current controllers", in *Industry Applications Conference and Thirty-Fourth IAS Annual Meeting Conference Record of the 1999 IEEE*, vol. 2, pp. 818-825.

[7] R. Teodorescu; F. Blaabjerg; M. Liserre and P.C. Loh "Proportional-resonant controllers and filters for grid-connected voltage-source converters", in *IEE Proceedings - Electric Power Applications*, vol. 153, iss. 5, pp. 750-762, 2006.

[8] Akagi H., "Active harmonic filters", *Proceedings of the IEEE*, vol. 93, iss. 12, pp. 2128-2141, 2005.

[9] Marco Liserre, Frede Blaabjerg, Steffan Hansen, "Design and Control of an LCL-Filter-Based Three-Phase Active Rectifier", *IEEE Trans. on Industry Application*, vol. 41, no. 5, pp. 1281-1291, 2005.